2024 IEEE International Conference on Robotics and Automation (ICRA 2024)
May 13-17, 2024. Yokohama, Japan

Lumped Parameter Dynamic Model of an Eversion Growing Robot: Analysis, Simulation and Experimental Validation

Panagiotis Vartholomeos[1], Zicong Wu[2], S.M.Hadi Sadati[2], and Christos Bergeles[2]

***Abstract*— This paper presents a lumped-parameter dynamic model of a pressure driven eversion robot carrying a catheter through its hollow core. A simulation framework based on the model is developed in MATLAB and is used for understanding the underlying physics, for identifying the regions of operation, and for demonstrating that, for a range of input commands, the catheter can be used as an actuation mechanism for propelling eversion; an approach especially useful for miniaturised systems. Simulations are experimentally validated on the MAMMOBOT system, which is a miniature steerable soft growing robot for early breast cancer detection. It was demonstrated that for most regions of operation experimental results compare well with simulation exhibiting an error less than 4%. Only one region of operation demonstrated larger deviations due possibly to unmodeled dynamics, which will be investigated in future work.**

I. INTRODUCTION

Researchers have recently developed eversion growing robots, also known as vine robots, inspired by the apical extension movement found in nature. Movement by apical extension is defined by lengthening of a body from a base with volume added almost exclusively at the most distal point. This behavior can be seen in nature in individual cells, such as pollen tubes and neurons, as well as at larger scales, in trailing vines [1], [2].

These robots exhibit movement of the most distal point without exerting any shear forces on the environment [1]–[4]. Due to this property and to the morphological adaptation to their environment, since they are soft and compliant, eversion growing robots lend themselves well to applications that involve navigation in confined spaces [5], such as archeological sites [6], disaster sites [7], and anatomical lumens [3], [4], [8]. In particular, in the medical domain, eversion growing robots have the potential to re-invent traditional micro-endoscopic technologies by offering a compelling solution that utilises tip eversion driven by internal pressure [3], [5] and performs safer navigation within sensitive lumen.

*This work has been funded by the European Union, under grant agreement No 101099145, project SoftReach, (https://softreach.eu/), and by Innovate UK under the Horizon Europe Guarantee Extension [10062486]. Z. Wu received support from China Scholarship Council (CSC No.:202008060101). For the purpose of open access, the author has applied for a CCBY licence to any Author Accepted Manuscript version arising from this submission.

[1]Panagiotis Vartholomeos is with the Department of Computer Science and Biomedical Informatics, University of Thessaly, Lamia, Greece. pvartholomeos@uth.gr

[2]Zicong Wu, S.M.Hadi Sadati and Christos Bergeles are with the School of Biomedical Engineering & Imaging Sciences, Kings College London, London, UK. {zicong.wu, smh_sadati, christos.bergeles}@kcl.ac.uk

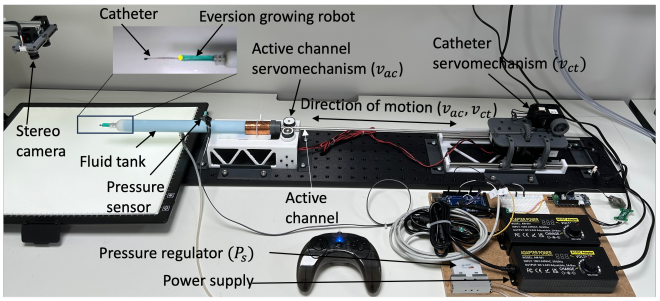

Fig. 1: MAMMOBOT eversion growing robot set-up [3], [4].

Mathematical modeling of eversion growing robots is a necessary tool for understanding their underlying physics and controlling their deployment. To this end, a quasi-static force balance model has been developed in [1], which leads to understanding of the movement and limitations of the apically extending robot. A quasistatic model was also developed in [9] to accurately position the end-effector. A dynamics simulator was presented in [10], [11], which can handle robot-object interactions in a cluttered environment. A nonlinear model predictive control in [12], was developed to guarantee the robot's control performance. A Finite Element Model (FEM) was developed in [4] which predicts the growing and interaction capabilities of a miniature eversion growing robot, but it is computationally expensive for real-time control. To the extent of the authors knowledge, no dynamic model has been developed so far for real-time control, taking into account the interaction with an integrated tool. The lack of models for dynamic control hinders the use of growing robots in tasks that require transmission of forces, such as minimally invasive surgery or maintenance and repair tasks, and limit their use to only inspection or diagnosis.

This paper proposes a dynamic model of an eversion growing robot, which accommodates in its hollow core an instrument, such as an optical fiber, an endoscope or a catheter. The contributions of the paper are: (i) a multiscale dynamic model, that captures transient responses relevant to large dimension systems, as well as stick-slip friction phenomena dominant to small scales such as millimeter diameter surgical endoscopes; (ii) the modeling of the interaction between the everting robot internal structure and the instrument passing through the robot's hollow core; (iii) a computationally efficient model that can be used for closed-loop control. The model is experimentally validated on the MAMMOBOT system shown in Fig (1), which is a soft growing robot being deployed for early breast cancer detection [2].

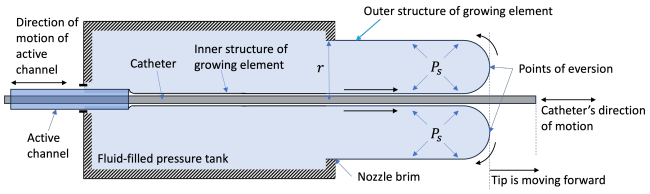

Fig. 2: Cross section of eversion growing robot.

II. DESCRIPTION OF THE ROBOTIC SYSTEM

The robot's hardware architecture is separated into two sub-systems: (1) subsystem for manipulation of the eversion growing element, and (2) subsystem for manipulation of a steerable catheter.

The first subsystem comprises a growing eversion element (a sheath) embedded in a pressurised fluid-filled tank, and an active channel for regulating the growing and retraction of the growing element alongside pressure control within the tank. The growing element is connected to the tank nozzle on one end, and to a stainless steel hollow tube, namely the "active channel", on the other end. As the growing element is pressurised, eversion is only possible with the simultaneous translation of the active channel. The latter is actuated by a servo system. The active channel, the growing element, and the fluid-filled tank are shown in Fig. (2). More information for the active channel functionality can be found in [3].

The second subsystem comprises a tendon-driven steerable catheter, fabricated by patterning NiTi tubing; a NiTi tendon to drive its deflection; a 3 degree of freedom (dof) servo system to enable the independent advancement, the deflection and the rotation of the steerable catheter. The element grows via tip eversion, i.e. rolling out, induced by its internal fluid pressure. The fluid tank is filled with saline and provides the necessary hydraulic pressure. The hardware components (actuators, sensors, controllers, communication boards) that realise this architecture are described in [3], [4].

In this work, the term growth refers to an increase in the length of the robot, and the term eversion refers to the process by which the material internal to the robot structure (inner structure in Fig. (2)) turns inside out and becomes part of the outside of the structure (outer structure in Fig. (2)). As pressure is applied internal to the robot, it pushes the tip forward. Since the outer structure is fixed and the inner structure is free to move forward, eversion of the inner structure occurs, adding new material to the tip and resulting in extension of the tip. Hence, in eversion growth, only the tip moves forward; there is no relative movement of the outer robot structure with respect to the environment.

III. PHYSICAL AND MATHEMATICAL MODEL

This section develops a dynamic model that can be used for analysis, synthesis and feedback control of the eversion growing robot. The model employs lumped parameter elements that represent the dominant dynamics of the system. The lumped parameter method was chosen because it leads to computationally efficient equations and can easily capture the dynamics of a mixed energy domain system (including mechanical, hydraulic, electrical subsystems) such as the one under study. Therefore the modeling method lends it self well for generating real-time, model-based control algorithms.

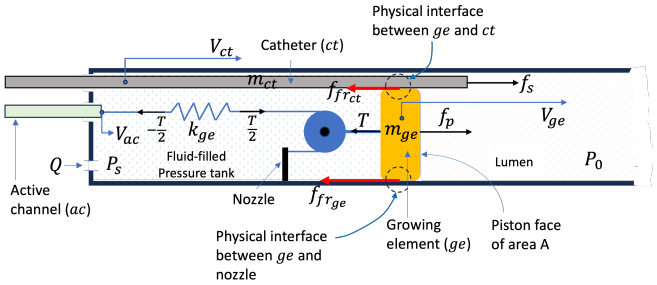

Fig. 3: Physical model of the eversion growing robot with catheter.

A. Physical Model

The physical model of the growing element dynamics is depicted in Fig. (3). The tip of the growing element is modelled as a plunger that converts hydraulic power from the fluid-filled tank, into mechanical power of the growing element tip. The plunger is connected to an ideal pulley, which in turn is connected to the active channel through a massless elastic string that represents the elasticity of the growing element's inner structure. One end of the string is connected to the active channel and the other to the tank's nozzle. Only tension forces can appear on the string; compression is impossible because it becomes slack. The pulley represents the kinematic relationship between the growing element inner structure and the tip, i.e. the tip velocity v_{ge} is half of that of the inner structure because of the eversion principle. The growing element has dynamics that are dominated by an apparent mass m_{ge} which represents the mass of the growing element material and any fluid mass in the lumen that is displaced as the tip expands.

The active channel velocity is controlled by a servo system which is non-backdrivable, i.e. the active channel can affect (limit) the speed of the growing element tip but the reverse is not true. Therefore, active channel velocity v_{ac} is considered as an ideal velocity source applied on one end of the string.

The catheter is modeled as a rod, of mass m_{ct}, in contact with the growing element tip (i.e. the plunger). The catheter speed v_{ct} is controlled by a servo system, also non-backdrivable. The catheter slides on plunger, which in turn slides on the nozzle of the tank. The friction force $f_{fr_{ct}}$ appears on the physical interface between the catheter and the plunger. The friction force $f_{fr_{ge}}$ appears on the physical interface between the inner and outer structures which come into contact at the nozzle brim; this contact is not depicted in Fig. (2). The force T is the total tension force exerted on the membrane. The tension on the inner and outer structure is equal to $f_k = \frac{T}{2}$ due to the pulley mechanism (half of the tension is transmitted to the active channel and the other half to the nozzle brim).

The force f_p is exerted on the plunger by the pressure in

the tank, and is given by

$$f_p = AP_s \tag{1}$$

where A is the face-area of the plunger. The force f_s is applied on the catheter by a servo actuator and is given by a closed-loop proportional control law of gain K_p:

$$f_s = K_p(v_{ct_{des}} - v_{ct}) \tag{2}$$

where velocity $v_{ct_{des}}$ is set to the servosystem as the desired velocity of the catheter.

The pressure regulator system is modeled as an ideal pressure source P_s to the fluid-filled tank. The reference pressure P_0 is the pressure in the lumen. The entire fluid-filled tank is always static and hence is considered as the inertial reference of the mechanical system ($v_0 = 0\ m/s$).

B. Mathematical Model

The authors opted for the Static-plus-Coulomb-plus-Viscous friction model given in (3) and depicted in Fig. (4). This static law of friction lends itself well for capturing the underlying physics of stick-slip phenomena for slowly varying velocity [14], [15], which is the case of the eversion growing robot. The friction law has been combined with a Karnopp velocity dead-band Δv to avoid chattering of the simulated response around zero velocity [13] and allow for fast simulations.

$$f_{fr} = \begin{cases} bv + F_C \operatorname{sgn}(v), & v \neq 0 \\ F_e, & v = 0,\ |F_e| < F_s \\ F_s \operatorname{sgn}(F_e), & v = 0,\ |F_e| \geq F_s \end{cases} \tag{3}$$

The parameter b, is the viscous friction coefficient, F_C is the Coulomb friction, and F_s is the breakaway force characterizing the limit between static friction and kinetic friction regime in Fig. (4). Since, these parameters depend on the nature of the physical interfaces onto which friction appears, they take different values at the interface between the growing element inner structure and the nozzle, and at the interface between the catheter and the inner structure. Friction force $f_{fr_{ct}}$ scales with the pressure P_s and with the contact area between the catheter and the growing element, which in turn depends on the length of eversion. However, in this paper, due to the small eversion length and relatively small pressure variations, these dependencies are neglected. The variable v is the relative velocity between the two surfaces, given by $v = v_{ge}$ for the interface between the growing element inner structure and the nozzle, and given by $v = v_{rel} = v_{ge} - v_{ct}$ for the interface between the growing element inner structure and the catheter.

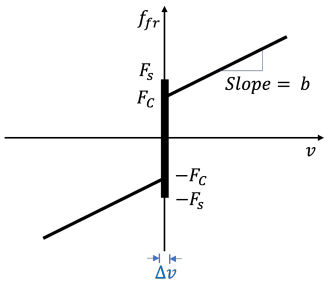

Fig. 4: Static-plus-Coulomb-plus-Viscous friction law.

According to (3), the friction forces exhibit jump-type discontinuities as a function of velocities v_{ge} and v_{rel}. These result in transitions (jumps) from static to kinetic states and vice versa, as shown in Table I. Each of these states is described by a different set of dynamic equations in state-space form, as explained next.

The state-space ODEs are derived according to the systematic approach of the Linear-Graph modeling method [16] or the Bond Graph method [17]. The state-space variables of the system are the v_{ge}, f_k and v_{ct} related to the three independent energy storage elements of the physical model in Fig. (3), namely the apparent mass m_{ge} of the growing element, the elasticity of the membrane of the growing element k_{ge} and the mass of the catheter m_{ct}.

TABLE I: Static and kinetic States of the system.

	$v_{rel} \approx 0$	$v_{rel} \neq 0$
$v_{ge} \approx 0$	State 1	State 2
$v_{ge} \neq 0$	State 3	State 4

State 1: The eversion growing element and the catheter are both static, i.e. $v_{ge} = v_{rel} = 0\ m/s$, and accelerations are zero too. This is expressed as:

$$\frac{d}{dt}\begin{bmatrix} v_{ge} \\ f_k \\ v_{ct} \end{bmatrix} = \begin{bmatrix} 0 \\ 0 \\ 0 \end{bmatrix} \tag{4}$$

The system behaves as a single body onto which the forces shown in Fig (5) are applied. It remains in State 1 as long as the forces exerted on the single body do not exceed the static friction limits, shown next.

$$f_s \leq |F_{S_{ct}}| \tag{5}$$

$$-f_k + f_p + f_s \leq |F_{S_{ge}}| \tag{6}$$

To avoid simulation chattering due to zero velocity detection, the algorithm sets $v_{ge} = v_{rel} = 0\ m/s$ whenever $v_{ge} \leq |\Delta v|$ and $v_{rel} \leq |\Delta v|$ respectively [13].

State 2: The growing element is not moving ($v_{ge} \leq |\Delta v|$). The catheter is moving at a velocity v_{ct}. The state-space equations are:

$$\frac{d}{dt}\begin{bmatrix} v_{ge} \\ f_k \\ v_{ct} \end{bmatrix} = \begin{bmatrix} 0 \\ 0 \\ \frac{1}{m_{ct}}(f_s - (b_{ct}v_{ct} + F_{C_{ct}} \operatorname{sgn}(v_{ct}))) \end{bmatrix} \tag{7}$$

When f_s is substituted by (2), Eq. (7) is written as:

$$\frac{d}{dt}\begin{bmatrix} v_{ge} \\ f_k \\ v_{ct} \end{bmatrix} = \begin{bmatrix} 0 & 0 & 0 \\ 0 & 0 & 0 \\ 0 & 0 & -\frac{(K_P + b_{ct})}{m_{ct}} \end{bmatrix} \begin{bmatrix} v_{ge} \\ f_k \\ v_{ct} \end{bmatrix} - \begin{bmatrix} 0 \\ 0 \\ \frac{1}{m_{ct}} \end{bmatrix} F_{C_{ct}} \operatorname{sgn}(v_{ct}) + \begin{bmatrix} 0 \\ 0 \\ \frac{K_p}{m_{ct}} \end{bmatrix} v_{ct_{des}} \tag{8}$$

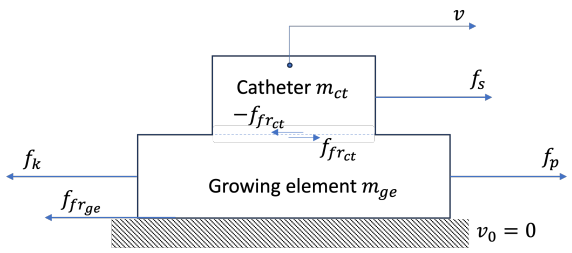

Fig. 5: Free body diagram of the single-body case.

State 3: In this state, the eversion growing element and the catheter exhibit stiction, i.e. one sticks onto the other due to growing element internal pressure. They move as a single body of mass $M = m_{ct} + m_{ge}$, having the same velocity v and the same acceleration $\frac{dv}{dt}$, as shown in Fig. (5). The single body behavior will be maintained as long as the interaction friction force $f_{fr_{ct}}$ is able to "hold together" the two-bodies. The state-space equations are given by:

$$\frac{d}{dt}\begin{bmatrix} v \\ f_k \end{bmatrix} = \begin{bmatrix} -\frac{b}{M} & -\frac{1}{M} \\ k_{ge} & 0 \end{bmatrix}\begin{bmatrix} v \\ f_k \end{bmatrix} - \begin{bmatrix} \frac{1}{M} \\ 0 \end{bmatrix} F_{C_{ge}} \operatorname{sgn}(v) + \begin{bmatrix} \frac{1}{M} \\ 0 \end{bmatrix} f_p + \begin{bmatrix} \frac{1}{M} \\ 0 \end{bmatrix} f_s \tag{9}$$

Substituting in (9), f_p and f_s by (1) and (2), results in

$$\frac{d}{dt}\begin{bmatrix} v \\ f_k \end{bmatrix} = \begin{bmatrix} -\frac{b+K_p}{M} & -\frac{1}{M} \\ k_{ge} & 0 \end{bmatrix}\begin{bmatrix} v \\ f_k \end{bmatrix} - \begin{bmatrix} \frac{1}{M} \\ 0 \end{bmatrix} F_{C_{ge}} \operatorname{sgn}(v) + \begin{bmatrix} \frac{A}{M} \\ 0 \end{bmatrix} P_s - \begin{bmatrix} \frac{1}{M} \\ 0 \end{bmatrix} K_p v_{ct_{des}} \tag{10}$$

To control the transition from State 3 to the other States, a condition that involves forces f_s and f_p is derived. The expression can be found by considering that the catheter, the growing element, and the single-body configuration of mass M, all exhibit the same acceleration. Then the following expressions hold:

$$\frac{dv}{dt} = \frac{dv_{ct}}{dt} = \frac{1}{m_{ct}}(f_s - f_{fr_{ct}}) \tag{11}$$

and

$$\frac{dv}{dt} = \frac{1}{M}(-bv - f_k + f_p + f_s - f_{fr_{ge}}) \tag{12}$$

Equating (11) and (12), substituting f_p and f_s by (1) and (2), and solving for $f_{fr_{ct}}$, yields:

$$\begin{aligned} f_{fr_{ct}} &= \frac{m_{ge}}{M} f_s - \frac{m_{ct}}{M}(f_p - f_k - bv - F_{C_{ge}} \operatorname{sgn}(v)) \\ &= -\frac{m_{ge}K_p + m_{ct}b}{M} v - \frac{m_{ct}}{M}(AP_s - f_k - F_{C_{ge}} \operatorname{sgn}(v)) + \frac{m_{ge}K_p}{M} v_{ct_{des}} \end{aligned} \tag{13}$$

Hence, the condition that the interaction force $f_{fr_{ct}}$ is able to "hold together" the two-bodies is given by:

$$-\frac{m_{ge}K_p + m_{ct}b}{M} v - \frac{m_{ct}}{M}(AP_s - f_k - F_{C_{ge}} \operatorname{sgn}(v)) + \frac{m_{ge}K_p}{M} v_{ct_{des}} \leq F_{S_{ct}} \tag{14}$$

State 4: The eversion growing element and the catheter are moving as two independent bodies. The state-space equations are given by:

$$\frac{d}{dt}\begin{bmatrix} v_{ge} \\ f_k \\ v_{ct} \end{bmatrix} = \begin{bmatrix} -\frac{(b+b_{ct})}{m_{ge}} & -\frac{1}{m_{ge}} & \frac{b_{ct}}{m_{ge}} \\ k_{ge} & 0 & 0 \\ \frac{b_{ct}}{m_{ct}} & 0 & -\frac{(K_P+b_{ct})}{m_{ct}} \end{bmatrix}\begin{bmatrix} v_{ge} \\ f_k \\ v_{ct} \end{bmatrix} + \begin{bmatrix} \frac{A}{m_{ge}} \\ 0 \\ 0 \end{bmatrix} P_s - \begin{bmatrix} \frac{F_{C_{ge}} \operatorname{sgn}(v_{ge}) - F_{C_{ct}} \operatorname{sgn}(v_{rel})}{m_{ge}} \\ 0 \\ \frac{-F_{C_{ct}} \operatorname{sgn}(v_{ct})}{m_{ct}} \end{bmatrix} - \begin{bmatrix} 0 \\ k_{ge} \\ 0 \end{bmatrix} v_{ac} + \begin{bmatrix} 0 \\ 0 \\ \frac{K_p}{m_{ct}} \end{bmatrix} v_{ct_{des}} \tag{15}$$

The catheter's viscous friction parameter b_{ct} is negligible compared to $F_{C_{ct}}$, and is ignored in the following analysis.

C. State-Transition Rules

Transitions from static conditions to kinetic conditions (e.g. $v_{ge} = 0 \rightarrow v_{ge} \neq 0$ or $v_{rel} = 0 \rightarrow v_{rel} \neq 0$) require to check when the breakaway friction forces $F_{S_{ct}}$ and $F_{S_{ge}}$ are overcome. For example, State 1 will transition to State 4 when (5) and (6) are not true. On the other hand, transitions from kinetic to static require the polling of velocities v_{ge} and v_{rel} and the triggering of state transitions when $v_{ge} < |\Delta v|$ or $v_{rel} < |\Delta v|$. Not all states transition to all other states. For example, State 2 cannot transition to State 3 directly, since the growing element has to accelerate first in order to reach a velocity $v_{ge} = v_{ct}$. Similarly, State 3, where the system acts as a single body, cannot transition to State 2 directly. The transition has to pass first from State 4, where the growing element and the catheter move as two independent bodies, before the growing element velocity decelerates to $v_{ge} = 0$. The transition rules are summarised in Table (II), where $v_{rel} \approx 0$ is equivalent to $v_{rel} < |\Delta v|$ and $v_{rel} \neq 0$ equivalent to $(v_{rel} < -\Delta v)$ & $(\Delta v < v_{rel})$. Equations (4)-(15) have been implemented in MATLAB and were numerically integrated using solver ODE 15s, for numerically stiff problems. The transition from one state to the other has been implemented using Event function which broadcasts interrupts when the conditions in Table (II) are met. These interrupts are responsible for the correct transition from one state to the other.

IV. Parameter Estimation and Model Validation

The experimental procedure is broken down into 2 parts. The first, focuses on the interaction of the eversion growing robot and the active channel. The exclusion of the catheter simplifies the experimental procedure because it allows examining the eversion principle only, having fewer parameters

TABLE II: Table of state transition rules.

Transitions	Conditions that trigger transition
A. $1 \rightarrow 2$	$(f_s > F_{S_{ct}}) \& (-f_k + f_p + F_{S_{ct}} < F_{S_{ge}})$
B. $1 \rightarrow 3$	$(-f_k + f_p + f_s > F_{S_{ge}})$ & $\left(-\frac{m_{ge}K_p + m_{ct}b}{M} v - \frac{m_{ct}}{M}(AP_s - f_k - F_C sgn(v)) + \frac{m_{ge}K_p}{M} v_{ct_{des}} \leq F_{S_{ct}}\right)$
C. $1 \rightarrow 4$	$(-f_k + f_p + f_s > F_{S_{ge}})$ & $\left(-\frac{m_{ge}K_p + m_{ct}b}{M} v - \frac{m_{ct}}{M}(AP_s - f_k - F_C sgn(v)) + \frac{m_{ge}K_p}{M} v_{ct_{des}} \geq F_{S_{ct}}\right)$
D. $2 \rightarrow 1$	$v_{rel} \approx 0$
E. $2 \rightarrow 4$	$(-f_k + f_p + F_{C_{ct}} > F_{S_{ge}})$
F. $3 \rightarrow 1$	$v = v_{ge} \approx 0$
G. $3 \rightarrow 4$	$\left(-\frac{m_{ge}K_p + m_{ct}b}{M} v - \frac{m_{ct}}{M}(AP_s - f_k - F_C sgn(v)) + \frac{m_{ge}K_p}{M} v_{ct_{des}} \geq F_{S_{ct}}\right)$
H. $4 \rightarrow 1$	$(v_{ge} \approx 0)$ & $(v_{rel} \approx 0)$
I. $4 \rightarrow 2$	$v_{ge} \approx 0$
J. $4 \rightarrow 3$	$v_{rel} \approx 0$

TABLE III: Simulation and experimental results.

	$v_{ac_1} = 5.8$ $[mm/s]$		$v_{ac_2} = 8.7$ $[mm/s]$		$v_{ac_3} = 11.6$ $[mm/s]$	
Pressure [kPa]	v_{ge} $[mm/s]$ Exp.	Sim.	v_{ge} $[mm/s]$ Exp.	Sim.	v_{ge} $[mm/s]$ Exp.	Sim.
110	0.05	0.0	0.28	0.0	0.1	0.0
115	0.25	0.3	0.2	0.3	1.0	0.3
120	2.3	1.1	3.3	1.1	5.4	1.1
125	2.7	1.85	4.0	1.85	5.1	1.85
130	2.9	2.6	4.3	2.6	5.5	2.6
135	2.9	2.9	4.4	3.4	5.6	3.4
140	2.9	2.9	4.4	4.15	6.2	4.15
145	3.1	2.9	4.5	4.35	5.8	5.7
150	3.1	2.9	4.5	4.35	5.9	5.7

to identify. The second experimental part is conducted using the complete system and demonstrates the effect of the catheter on the growing element response.

A. Part 1: Growing element and active channel interaction

1) Parameter estimation: In order to identify the friction model, two different experiments were conducted. The first was used to find the breakaway friction force $F_{S_{ge}}$, while the second to yield the kinetic friction parameters $F_{C_{ge}}$ and viscous friction coefficient b. These experiments provided an initial gross estimate, which was subsequently fined-tuned manually by comparing simulation and experimental results.

In the first experiment, the pressure P_s was gradually increased until growing element tip motion was detected. This breakaway motion was achieved for pressure values $P_s = 115kPa$.

In the second experiment, tests were conducted for 9 pressure values $P_s[kPa]$: $\{110, 115, 120, 125, 130, 135, 140, 145, 150\}$, and at active channel velocity $v_1 = 5.8mm/s$. The experimental procedure involved 3 steps: (1) the pressure regulator generates desired pressure P_s in the tank; (2) then the active channel servomechanism moves forward the channel at the desired speed v_{ac}; (3) the camera records the motion of the everting robot tip. The experimental results for parameter estimation are presented in the first column of Table (III). Using the measured v_{ge} values for pressures $P_s = 120kPa$, $P_s = 125kPa$ and $P_s = 130kPa$ for $v_{ac_1} = 5.8mm/s$, the values of viscous friction parameter b and the Coulomb level $F_{C_{ge}}$ were estimated.

The dynamic parameters m_{ge}, k_{ge}, cannot be captured by the sensors of the set-up (would require high speed camera and strain gauges), and were obtained from the data sheets for the LDPE film of the growing element material [3]. The geometric parameter of face-area A was obtained from the CAD model o MAMMOBOT [3]. Estimated and measured parameter values are presented in Table (IV).

TABLE IV: Estimated parameters. System without catheter.

Parameter	Value	Parameter	Value
m_{ge}	$0.5\ 10^{-14}\ kg$	$F_{S_{ge}}$	$11.7\ N$
k_{ge}	$5\ 10^{5}\ N/m$	$F_{C_{ge}}$	$9.125\ N$
A	$10^{-4}\ m^2$	b	$1250\ Ns/m$

2) Model validation: Two additional sets of experiments were conducted for pressure values $P_s = \{110, 115, 120, 125, 130, 135, 140, 145, 150\}$ $[kPa]$, and for active channel velocities $v_{ac_2} = 8.7\ mm/s$, $v_{ac_3} = 11.6\ mm/s$. A comparison of experimental and simulation results is presented in Table (V). It is reminded that the v_{ge} is the velocity of the growing element tip, which due to eversion is *half of the speed* of the growing element.

An examination of experimental and simulation results reveals that the growing element exhibits two regions of operation. The first occurs when the growing element velocity is $v_{ge} < \frac{v_{ac}}{2}$ (cells in blue). The second region of operation occurs when $v_{ge} \approx \frac{v_{ac}}{2}$ (cells in green). In the latter case, the growing element has sufficient pressure to reach velocities greater than v_{ac} but fails to do so because it is constrained by its connection to the active channel. Operating in the green region is advantageous because it ensures the growing element acquires always the active channel speed. In the green regions the steady state values are predicted accurately by the simulation (error less than 5%). However, the pressure at which the system enters the green region deviates (10kPa higher) with respect to experimental results (error 10%).

It is observed that in the blue region, in Table (III), there is a large discrepancy (error 30%) between the predicted and the actual v_{ge}, which, interestingly, becomes greater as the active channel velocity becomes higher. This discrepancy is possibly due to unmodeled dynamics, which are triggered by the active channel's forward motion; as the active channel

displaces fluid in the tank it imparts an additional force on the growing element which results in velocities greater than the predicted ones. If used appropriately, these dynamics could act as an auxiliary driving force in low pressures; a feature that would lend it self well in miniaturised designs, where the allowable tank-pressures are limited. Finally, for pressures $P_s < 115kPa$ the system is static (cells in yellow). This is accurately predicted by simulation.

B. System with the catheter

Experiments were conducted, following same procedure as in previous section, for estimating the static and kinetic friction coefficients and K_p. The parameter m_{ct} was calculated based on the CAD model of the catheter. All parameters are presented in Table (V).

TABLE V: Estimated parameters related to the catheter.

Parameter	Value	Parameter	Value
$F_{S_{ct}}$	$6.05\ N$	$F_{C_{ct}}$	$5.5\ N$
m_{ct}	$5 \cdot 10^{-4}\ kg$	K_p	$5 \cdot 10^4$

Simulations and experiments were conducted, for the complete system with the catheter, for model validation purposes. The following catheter velocities were tested: $\{0,\ 1.4,\ 2.1,\ 2.9,\ 3.6,\ 4.3\}\ mm/s$. Tank pressure was set equal to $P_s = 110\ kPa$ and active channel speed was set equal to $v_{ac} = 5.8\ mm/s$. Experimental and simulation results are compared in Table (VI).

TABLE VI: Simulation and experimental results of the complete system.

	Growing tip velocity v_{ge} [mm/s]	
Catheter velocity [mm/s]	Exp.	Sim.
0.0	0.0	0.0
1.8	0.9	0.9
2.9	1.3	1.45
3.9	1.8	1.9
4.8	2.2	2.35
6.3	2.8	2.9

Simulation results are in accordance with experimental results (exhibit error less than 4%). The first simulation demonstrates that a zero-velocity catheter adds friction to the system and becomes a barrier to the eversion process. Hence, for relatively small pressures such as $P_s = 110\ kPa$ eversion is inhibited and $v_{ge} = 0\ m/s$. On the contrary, when the catheter is sliding and $v_{rel} \leq 0$, then friction $f_{C_{ct}}$ assists eversion, as demonstrated by the simulations and the experiments, and is inferred by (15). Hence, catheter's controlled motion can be used as an actuation mechanism for propelling eversion; an approach especially useful when miniaturising an eversion growing robot where friction forces become larger than pressure forces.

For non-zero catheter velocity, simulation results predict that the system operates in State 3 or State 4, where as

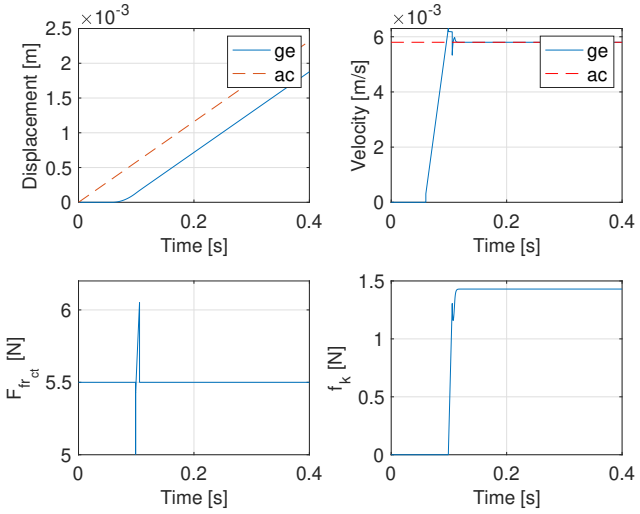

Fig. 6: Simulation results for $v_{ac} = 5.8\ mm/s$, $P_s = 110\ kPa$ and $v_{ct} = 6.3\ m/s$.

expected, $v_{ge} \leq \frac{v_{ct}}{2}$ due to the eversion mechanism. Interestingly, this does not hold in the last simulation. In that case, the value of v_{ge} is equal to $\frac{v_{ac}}{2} = 2.9\ mm/s$. This happens because $v_{ac} < v_{ct}$, and thus the active channel restrains the tip-eversion velocity to the value $\frac{v_{ac}}{2}$. The predicted values for inner structure tension f_k, for tip velocity v_{ge} and displacement x_{ge}, and friction force $f_{fr_{ct}}$ are presented in Fig. (6). The simulation steps are described next.

At time $t = 0\ s$ the catheter velocity is $v_{ct} = 6.3\ m/s$. Pressure is gradually increasing at a rate $10^6 \cdot t$, where t is the time. This ramp input was generated for demonstrating the transition through different states of operation. At $t = 0.06\ s$ the system transitions from state 2 (since $v_{rel} \neq 0$) to state 4, i.e. $v_{ge} \neq 0$ and $v_{rel} \neq 0$. At $t = 0.1\ s$ the system briefly exhibits state 3, i.e. $v_{ge} \neq 0$ and $v_{rel} = 0$. At time $t = 0.106\ s$. friction $f_{fr_{ct}}$ at the interface reaches the static limit $F_{S_{ct}} = 6.05\ N$ and catheter breaks away from growing element; the system returns to state 4.

Simulation time is three times the actual time. However, simulation runs on a MATLAB environment which uses an interpreter during code execution. If the same code is implemented in C/C++ a speed improvement by a factor of 10 is expected.

V. CONCLUSION

This paper presented a lumped-parameter dynamic model of a pressure driven eversion robot carrying a catheter through its hollow core. A simulation framework was developed in MATLAB and was experimentally validated on the MAMMOBOT system. Through a sequence of simulations the underlying physics were studied, the subsystems interaction was investigated, and the effect of the catheter's motion passing through the growing element was studied, and was demonstrated that it can be used as an actuation mechanism for propelling eversion.

REFERENCES

[1] Blumenschein, L.H., Okamura, A.M., Hawkes, E.W. (2017). Modeling of Bioinspired Apical Extension in a Soft Robot. In: Mangan, M., Cutkosky, M., Mura, A., Verschure, P., Prescott, T., Lepora, N. (eds) Biomimetic and Biohybrid Systems. Living Machines 2017. Lecture Notes in Computer Science(), vol 10384. Springer, Cham. https://doi.org/10.1007/978-3-319-63537-8_45

[2] Blumenschein Laura H., Coad Margaret M., Haggerty David A., Okamura Allison M., Hawkes Elliot W., "Design, Modeling, Control, and Application of Everting Vine Robots", Frontiers in Robotics and AI, V7, 2020, DOI=10.3389/frobt.2020.548266.

[3] P. Berthet-Rayne et al., "MAMMOBOT: A Miniature Steerable Soft Growing Robot for Early Breast Cancer Detection," in IEEE Robotics and Automation Letters, vol. 6, no. 3, pp. 5056-5063, July 2021, doi: 10.1109/LRA.2021.3068676.

[4] Wu Z, De Iturrate Reyzabal M, Sadati SMH, Liu H, Ourselin S, Leff D, Katzschmann RK, Rhode K, Bergeles C. Towards A Physics-based Model for Steerable Eversion Growing Robots. IEEE Robot Autom Lett. 2023 Feb;8(2):1005-1012. doi: 10.1109/LRA.2023.3234823. PMID: 36733442; PMCID: PMC7614130.

[5] E. W. Hawkes, L. H. Blumenschein, J. D. Greer, and A. M. Okamura, "A soft robot that navigates its environment through growth," Science Robotics, vol. 2, no. 8, 2017.

[6] M. M. Coad, L. H. Blumenschein, S. Cutler, J. A. R. Zepeda, N. D. Naclerio, H. El-Hussieny, U. Mehmood, J.-H. Ryu, E. W. Hawkes, and A. M. Okamura, "Vine robots: Design, teleoperation, and deployment for navigation and exploration," IEEE Robotics & Automation Magazine, vol. 27, no. 3, pp. 120–132, 2019.

[7] V. Sikhin and S. Harikrishnan, "Human detection system for rescue operations," in AIP Conference Proceedings, vol. 2222, no. 1. AIP Publishing LLC, 2020, p. 040021.

[8] M. Li, R. Obregon, J. J. Heit, A. Norbash, E. W. Hawkes, and T. K. Morimoto, "Vine catheter for endovascular surgery," IEEE Transactions on Medical Robotics and Bionics, vol. 3, no. 2, pp. 384–391, 2021.

[9] C. Tutcu, B. A. Baydere, S. K. Talas, and E. Samur, "Quasi-static modeling of a novel growing soft-continuum robot," The International Journal of Robotics Research, vol. 40, no. 1, pp. 86–98, 2021.

[10] R. Jitosho, N. Agharese, A. Okamura and Z. Manchester, "A Dynamics Simulator for Soft Growing Robots," International Conference on Robotics and Automation (ICRA), 2021, doi: 10.1109/ICRA48506.2021.9561420.

[11] D. A. Haggerty, N. D. Naclerio, and E. W. Hawkes, "Characterizing environmental interactions for soft growing robots," in 2019 IEEE/RSJ International Conference on Intelligent Robots and Systems (IROS). IEEE, 2019, pp. 3335–3342.

[12] H. El-Hussieny, I. A. Hameed, and J.-H. Ryu, "Nonlinear model predictive growth control of a class of plant-inspired soft growing robots," IEEE Access, vol. 8, pp. 214 495–214 503, 2020.

[13] Karnopp, D. (March 1, 1985). "Computer Simulation of Stick-Slip Friction in Mechanical Dynamic Systems." ASME. J. Dyn. Sys., Meas., Control. March 1985; 107(1): 100–103. https://doi.org/10.1115/1.3140698

[14] Henrik, Olsson., Karl, Johan, Åström., Carlos, Canudas, de, Wit., Magnus, Gäfvert., P., Lischinsky. (1998). Friction Models and Friction Compensation. European Journal of Control, 4(3):176-195. doi: 10.1016/S0947-3580(98)70113-X

[15] E. G. Papadopoulos and G. C. Chasparis, "Analysis and model-based control of servomechanisms with friction," IEEE/RSJ International Conference on Intelligent Robots and Systems, Lausanne, Switzerland, 2002, pp. 2109-2114 vol.3, doi: 10.1109/IRDS.2002.1041578.

[16] Derek Rowell, David Wormley, "System Dynamics: An introduction", Pearson; 1st edition (September 30, 1996).

[17] Dean C. Karnopp, Donald L. Margolis, Ronald C. Rosenberg, "System Dynamics: Modeling, Simulation and Control", John Wiley and Sons, Inc., 5th edition, 2012.